Bioactive Materials 17 (2022) 162–177

Contents lists available at ScienceDirect

Bioactive Materials

journal homepage: www.keaipublishing.com/en/journals/bioactive-materials

Bio-inspired, bio-degradable adenosine 5′-diphosphate-modified hyaluronic acid coordinated hydrophobic undecanal-modified chitosan for hemostasis and wound healing

Yihao Liu [a,1], Haoyi Niu [a,***,1], Chengwei Wang [a,****,1], Xiaoxiao Yang [c], Wentao Li [a], Yuxin Zhang [a], Xiaojun Ma [e], Yuanjing Xu [d], Pengfei Zheng [b,**], Jinwu Wang [a,d,*], Kerong Dai [a,d]

[a] Shanghai Key Laboratory of Orthopedic Implant, Department of Orthopedic Surgery, Shanghai Ninth People's Hospital, Shanghai Jiao Tong University School of Medicine, No. 639 Zhizaoju Rd, Shanghai, 200011, China
[b] Department of Orthopaedic Surgery, Children's Hospital of Nanjing Medical University, No. 72 Guangzhou Rd, Nanjing, 210008, China
[c] Department of Rehabilitation, Huashan Hospital, Fudan University, No.12 Middle Urumqi Rd, Shanghai, 200040, China
[d] Med-X Research Institute, School of Biomedical Engineering, Shanghai Jiao Tong University, No. 1956 Huashan Rd, Shanghai, 200030, China
[e] Department of Orthopedics, Shanghai General Hospital, Shanghai Jiao Tong University School of Medicine, No. 85 Wujin Rd, Shanghai, 200080, China

ARTICLE INFO

Keywords:
Hemostasis
Antibacterial
Wound healing
Hyaluronic acid
Chitosan

ABSTRACT

Uncontrolled hemorrhage and wound infection are crucial causes of trauma-associated death in both the military and the clinic. Therefore, developing an efficient and rapid hemostatic method with biocompatibility, easy degradation, and wound healing is of great importance and desirability. Inspired by spontaneous blood cell plug formation in the hemostasis process, an adenosine 5′-diphosphate modified pro-coagulation hyaluronic acid (HA-ADP) coordinated with enhanced antibacterial activity of undecanal-modified chitosan (UCS) was fabricated through physical electrostatic cross-linking and freeze-drying. The as-prepared hydrogel sponges showed a porous structure suitable for blood cell adhesion. In particular, the hydrogel exhibited excellent antibacterial ability and promoted the adhesion of platelets and red blood cells, thus inducing a prominent pro-coagulation ability via platelet activation, which exhibits a shorter hemostasis time (58.94% of control) *in vitro*. Compared with commercially available CELOX and gelatin sponge (GS), HA-ADP/UCS accelerates hemostasis and reduces blood loss in both rat tail amputation and rat artery injury models. Furthermore, all the samples exhibited superior cytocompatibility and biodegradability. Due to these performances, HA-ADP/UCS promoted full-thickness skin defect healing significantly *in vivo*. All the properties of HA-ADP/UCS suggest that it has great potential for translation as a clinical application material for hemostatic and wound healing.

1. Introduction

Uncontrolled bleeding is a crucial cause of trauma-associated death not only in the military but also in the clinic [1,2]. Thus, timely on-site hemostasis by using first-aid hemostatic materials plays a crucial role in saving an injured individual's life [2]. However, using standard gauze dressing to directly press the wound area is still the main method to deal with blood loss in emergencies [3], which often requires further treatment of the secondary wound damage and delays the wound healing process. Therefore, an ideal on-site first-aid hemostatic material should exhibit efficient and rapid hemostasis performance, great biocompatibility, easy degeneration without further processing, and promotion of wound healing [1,4,5]. Although hemostatic materials, such as keratin sponge [6], gelatin sponge [1], and nano-clay [7] have been developed

Peer review under responsibility of KeAi Communications Co., Ltd.
* Corresponding authorShanghai Key Laboratory of Orthopedic Implant, Department of Orthopedic Surgery, Shanghai Ninth People's Hospital, Shanghai Jiao Tong University School of Medicine, No. 639 Zhizaoju Rd, Shanghai, 200011, China.
** Corresponding author.
*** Corresponding author.
**** Corresponding author.
E-mail address: wangjw-team@shsmu.edu.cn (J. Wang).
[1] Y.L. and H.N. and C.W. contributed equally to the work.

https://doi.org/10.1016/j.bioactmat.2022.01.025
Received 4 November 2021; Received in revised form 13 January 2022; Accepted 13 January 2022
Available online 29 January 2022

over the past decades, and some have even been transformed to be commercially available, such as QuikClot powder and HemCon dressing, they often present undesired hemostatic performance [8]. Therefore, it remains challenging to develop an efficient and rapid hemostatic material that is biocompatible, easy to degrade, and promotes wound healing.

Hydrogel sponges possess a porous structure that supports their high hygroscopicity to induce blood component concentration and adhesion, and eventually promote blood coagulation [2,5]. Additionally, the connected structure of hydrogel sponges permits gas permeability, forms an anti-infective barrier, absorbs wound effusion, and preserves a suitable humid environment [9,10]. Therefore, hydrogel sponges could be suitable as first-aid hemostatic materials. Generally, hydrogel sponges are fabricated by freeze-drying that followed by chemical or physical crosslinking [11]. Comparably, physical gelation has been developed via hydrogen bonding or electronic interaction [12–14], which avoids the addition of organic cross-linkers or catalysts, and eliminates unnecessary cytotoxicity functional group introduction in the process of chemical gelation, which displays promising compatibility [11,15]. Furthermore, physical gelation via electronic interaction could be a promising method for the large-scale synthesis of hydrogels just by mixing anionic components with cationic partners.

Hyaluronic acid (HA) is an anionic glycosaminoglycan in the extracellular matrix, which accounts for ~50% of the total HAs distributed in the skin [16]. Additionally, the chemical structure of HA contains an abundant carboxyl group that endows HA with the feasibility of conjugation and modification. Recently, various HA derivatives have been exploited and used for tissue repair and regeneration because of the excellent cytocompatibility of HA, which can promote cell adhesion, proliferation, and migration [14,16,17]. Adenosine 5′-diphosphate (ADP), a physiologically relevant platelet agonist, is stored in the dense granules of platelets [18]. During the spontaneous hemostasis process, ADP is released from the dense granules of platelets and facilitates many positive feedback cascades that facilitate platelet aggregation and promote thrombus formation and stabilization [19,20]. Although ADP has great pro-coagulation potential [19], there are very few reports about ADP-modified materials as hemostatic. Thus, the ADP-modified HA could have great potential for platelet activation to facilitate blood coagulation, which is used as a first-aid hemostatic.

Chitosan (CS) is a positively charged polymer that is derived from chitin by varying the acetamide groups into primary amino groups, which can form an electronic interaction with electronegative membranes of blood cells and consequently advance blood cell aggregation, thus enabling CS with the ability of pro-coagulation [14,21]. However, pristine CS alone cannot achieve excellent hemostatic performance. Various modified CS materials have been developed to improve the pro-coagulation properties of CS [2,22]. Especially, hydrophobically modified CS (hm-CS) can form strong interaction with blood cells that promote blood cells immobilization, aggregation, and clotting due to its hydrophobic interaction capability, besides the hm-CS also pose similar properties of CS such as cytocompatibility, biodegradation and antibacterial effect [23]. Additionally, hm-CS can not only kill bacteria but also capture bacteria by inserting the hydrophobic group of hm-CS into the lipid bilayer of the outer membrane of microbes [24]. Therefore, hm-CS would be another candidate for electrostatic crosslinking hydrogel sponge preparation.

In this study, we endeavored to develop HA-ADP coordinated with UCS, a hm-CS, hydrogel sponge for rapid hemostasis and wound healing. The material was fabricated via electrostatic interactions crosslinking method, followed by freeze-drying. Furthermore, the UCS can not only facilitate blood cell aggregation through electrostatic interactions but also disrupt bacterial function. Furthermore, the HA-ADP facilitated platelet activation and plug formation. The potential of HA-ADP/UCS as a hemostatic material was tested in terms of its physicochemical qualities, morphologies, and *in vitro* antibacterial and hemostatic properties. Grave extremity hemorrhage in rat-tail amputation/rat-artery injury models and a full-thickness skin defect model with bacterial infection were used to test hemostatic and wound healing performance *in vivo*. The cytocompatibility and safety of these samples were also examined via CCK8, live/dead staining, and hemolysis tests *in vitro*. Biodegradable performance was also assessed both *in vitro* and *in vivo*.

2. Materials and methods

2.1. Materials

Hyaluronic acid (HA, Mw 35KD, Shanghai Yuanye Biotechnology Co. Ltd), Chitosan (CS, 50,000–190,000 Da, deacetylation 75–85%, Sigma-Aldrich), Adenosine 5′-diphosphate sodium salt (ADP, Shanghai Aladdin Industrial Co. Ltd.), Sodium cyanoborohydride ($NaBH_3CN$, Shanghai Aladdin Industrial Co. Ltd.), Undecanal (UDA, Shanghai Aladdin Industrial Co. Ltd.), *N*-(3-Dimethylaminopropyl)-*N*′-ethyl carbodiimide hydrochloride (EDC, Shanghai Aladdin Industrial Co. Ltd.), *N*-Hydroxysuccinimide (NHS, Shanghai Aladdin Industrial Co. Ltd.), Gelatin Sponge (GS, Xiang'en Jiangxi Medical Technology Development Co. Ltd), CELOX hemostatic granules, Cell Counting Kit-8 (CCK8, Dojindo (Shanghai) Co. Ltd.), LDH Kit (Dojindo (Shanghai) Co. Ltd.), Enzyme-Linked Immunosorbent Assay Kits (ELISA, Hangzhou Multi Sciences (LIANKE) Biotech Co. Ltd.).

2.2. Synthesis of ADP-Modified hyaluronic acid

HA-ADP was prepared via ADP's conjugation to HA (Table S1). Briefly, 1 g of HA was dissolved in 100 mL deionized water (DW) and the pH of the solution was ~5.5 adjusted by using 1 M HCl and 1 M NaOH. Thereafter, the synthesis system was catalyzed with 0.1712 g EDC and 0.1026 g NHS under stirred vigorously for 20 min and then adding an amount of 0.3500 g ADP with another 24 h stirring. The above solution was subsequently purified via dialysis (cut-off 3500) against DW (changed every 12 h) for 72 h. The as-prepared HA-ADP was dried by lyophilization and stored for further use.

2.3. Synthesis of undecanal-modified chitosan

UCS was synthesized as previous reports (Table S2) [23,25]. In brief, 1 g of CS was completely dissolved in 100 mL of 0.05 M HCl, adjusting the pH of the solution to 5.5 by using 1 M NaOH. After that, the solution of the 100 μL undecanal in 10 mL ethanol was added into CS solution and stirred for 1 h. An excess of $NaBH_3CN$ was then mixed into the above solution and stirred at 25 °C for 24 h. The as-prepared UCS was also purified via dialysis (cut-off 3500) against DW (changed every 12 h) for 72 h and collected by lyophilized.

2.4. HA-ADP/UCS hydrogel sponge preparation

The HA-ADP/UCS hydrogel was prepared via simple mixing. Briefly, 1 mL of 1% (w/v) HA-ADP solution and 1 mL of 1% (w/v) UCS solution were added into the same plastic tube, mingled vigorously, and quickly transferred into liquid N_2. After that, the as-prepared HA-ADP/UCS hydrogel was lyophilized to produce HA-ADP/UCS hydrogel Sponge. Additionally, HA/CS and HA/UCS were also prepared as control sponges by using the same producer.

2.5. Characterization

2.5.1. FTIR and NMR

The chemical structure of HA-ADP and UCS was characterized via nuclear magnetic resonance (NMR) spectroscopy on a Bruker Avance NEO 600 MHz spectrometer and FTIR on Nicolet 6700 FTIR spectrometer. All samples for ^1H NMR spectrum were obtained by testing the NMR tube that contained the solution of samples, and for FTIR were handled via the attenuated total reflectance (ATR) approach.

2.5.2. Rheological and morphology studies

To confirm the cross-linking between HA-ADP and UCS, the as-prepared samples' frequency-dependent rheological properties were examined with a strain of 1% at 37 °C. The storage modulus (G′) and loss modulus (G″) were recorded. The micro morphologies of the hydrogel sponge were observed by using scanning electron microscopy (SEM, SIRION 200, America). The surface of the HA-ADP/UCS hydrogel was observed by SEM after spraying with gold.

2.5.3. Determination of swelling ratio

The as-prepared samples' equilibrium swelling ratio was assessed by the reported method with some modifications [1,26]. All pre-dried samples (W_0) were put in strainers and weighed (W_d). Then, all samples with strainers were placed into a 6-well cell culture plate that contained excessive DW or PBS (pH 7.4). Thereafter, the samples with strainers were taken out after 30 s, 1 min, 2 mins, 5 mins, 8 mins and 10 min and removed the excess liquid by lightly dabbing on filter papers, the weight of wetting samples with dried strainers was recorded as W_t. And the swelling ratio was computed as the following Eq: Swelling ratio (%) = $((W_t - W_d)/W_0) \times 100\%$

2.5.4. Contact angle studies

To confirm the hydrophobicity of CS, UCS and the as-prepared samples, the contact angles were examined. In brief, 60 mg CS, UCS, HA/CS, HA/UCS and HA-ADP/UCS were weighed and tableted by tablet compressing machine to obtain regular surfaces. Then, the contact angles were examined by Contact Angle Meter (JC2000D1, POWEREACH, China).

2.5.5. Zeta potential

To demonstrate the crosslink between HA groups (HA, HA-ADP) and CS groups (CS, UCS) through electronic interaction and the alteration of the electronic interactions after HA and CS modified by ADP and UDA, respectively, the zeta potentials were tested. In brief, 1% (w/v) HA, HA-ADP, CS and UCS were solved in DW and the pH was adjusted to ~5.5 by using 1 M HCl and 1 M NaOH. The zeta potentials were tested by Nano-sized Zeta potentiometer (Zetasizer Nano-ZS90, Malvern, UK) and each group was repeated for three times.

2.5.6. In vitro and in vivo degradation

As reported by preceding reports, *in vitro* degradation tests were implemented in simulated body fluid (SBF, pH 7.4) [5]. In brief, 20 mg of specimens (W_0) was soaked in 2 mL of SBF, pH 7.4 with shaking at 37 °C and 60 rpm. At each set timepoint, all specimens were centrifugated collection and washed several times with DW and followed by freeze-drying and weighing (W_t). The percentage of degradation at each timepoint was computed by the Eq: (WL (%) = $((W_0 - W_t)/W_0) \times 100\%$).

20 mg samples were implanted under SD rats' dorsal skin for degradation test *in vivo*. After 10, 20 and 30 days, the implanted regions' tissue was sheared meticulously and managed with 4% paraformaldehyde solution. The wound tissue's pathological segment was then analyzed through H & E staining and imaged (Pannoramic DESK, 3D Histech, Hungary).

2.6. Cytocompatibility

2.6.1. CCK-8 assay

The cytocompatibility of samples was assessed by CCK8 assay by using REPC (Rat Endothelial Progenitor Cells) and HUVEC (Human Umbilical Vein Endothelial Cells) as model cells. Briefly, the cells were added into 96-well plates with a density of 8000 cells per well for 12 h. After that, the original DMEM was changed to the extraction of samples (0.1 g/mL DMED), and the DMEM medium alone was used as a control. Then, the cells were cultured at 5% CO_2, 37 °C atmospheres for 1/4/7 days. Subsequently, the cell viability was assessed via CCK8 by detecting the optical density at 450 nm that was measured using a microplate reader (Infinite M200 Pro, Tecan). Each group's relative growth rate (RGR) was calculated by the following Eq: RGR = $(OD_{(Experiment - Blank)}/OD_{(Control-Blank)}) \times 100\%$.

2.6.2. Live/dead staining assay

The morphologies of REPC and HUVEC that direct contact with samples were characterized by Live/Dead staining assay. Briefly, 10 mg of samples were placed into 35 mm glass-bottom dishes and sterilized by UV irradiation. Around 100000 cells were then inoculated onto the soaked samples' surface, culturing at 37 °C and 5% CO_2 atmosphere for 24 h and 72 h respectively. Afterward, each well was stained by Live/Dead Staining Kit according to the manufacturer's instructions. A confocal microscope (Leica Microsystems Inc., USA) was used for capturing the fluorescence images of cell adhesion and viability.

2.6.3. Hemolysis

As in previous reports, hemolysis assay was conducted with some changes [1,8]. Citrated whole blood (CWB) from New Zealand White Rabbit was collected with a blood/3.8% sodium citrate solution (9:1). 50 μL of CWB was then mixed into 1 mL PBS that contained 10 mg of sample. Positive and negative control used DW and PBS, respectively. After being cultivating at 37 °C for 1 h, the mixture was centrifuged at 3000 rpm for 5 min, and the absorbance of the supernatant liquid was measured at 540 nm. The hemolysis ratio was assessed by the Eq: Hemolysis (%) = ((sample abs 540 nm – negative control abs 540 nm)/(positive control abs 540 nm – negative control abs 540 nm)) × 100%

2.6.4. Assessment of IL-6 and TNF-α by ELISA

The IL-6 and TNF-α level of samples was assessed by rat ELISA kits by using REPC as model cells. Briefly, 10 mg of samples were placed into 12-well plate and sterilized by UV irradiation. Around 100000 cells with 1 mL DMEM medium were then added into each well soaking samples' surface, culturing at 37 °C and 5% CO_2 atmosphere for 3 days. Afterward, each well was measured by IL-6 and TNF-α ELISA Kit according to the manufacturer's instructions. The results were evaluated by detecting at 450 nm (630 nm as reference) using a microplate reader (Infinite M200 Pro, Tecan).

2.7. Antibacterial performance

2.7.1. Bacteria culture

The gram-negative *Escherichia coli* (*E. coli*, ATCC 25922), gram-positive *Staphylococcus aureus* (*S. aureus*, ATCC 25923) and gram-positive Methicillin-resistant *Staphylococcus aureus* (MRSA, ATCC 43300) were used to evaluate the antibacterial performance of all samples. Briefly, 100 μL stock bacteria were added into 5 mL of sterilized fresh LB liquid medium and cultivated at 37 °C for 6–8 h. Then, the concentration of bacterial suspensions was measured by utilizing a multifunctional microplate reader (Infinite M200 Pro, Tecan) at 625 nm.

2.7.2. In vitro antibacterial performance

Typically, 10 μL of 1×10^8 colony-forming units/mL (CFU/mL) bacterial solution was added onto the surface of 10 mg sterilized samples, and 10 μL of the bacterial solution alone was used as control. 1 mL of aseptic PBS was added to suspend residual bacteria after 2 h incubation at 37 °C. Surviving bacteria colony was assessed by observing a standard agar plate onto which was dropped 10 μL resuspension and then cultured for another 24 h at 37 °C. To count the surviving bacteria colony, various 10-fold gradient dilutions in aseptic PBS were spread onto agar plates and the survivors were obtained through images of plates after cultured. Each group was repeated three times, and the killing rate was calculated by the following Eq: Killing rate (%) = ((germs count of control - survivor count of the sample)/germs counts of control) × 100%.

Additionally, the morphology of bacterial was also observed by using

a scanning electronic microscope (SEM). Briefly, 1 mL of 5 × 10^6 bacterial solutions was co-cultured with each sterilized sample. After 2 h, the sample was rinsed three times with sterilized PBS after bacteria suspension removing, subsequently, the sample was fixed with 2.5% glutaric dialdehyde solution and dehydrated with a gradient ethyl alcohol solution. Finally, the samples were freeze-dried, gold sputtering, and observed by using SEM.

2.8. In vitro and in vivo hemostasis properties

2.8.1. Blood colt index

The blood clotting test was adapted from previous reports with some changes [1,4]. 100 μL of CWB was dropped onto the prewarmed sample's surface and incubated for 15 min at 37 °C. Then, free red blood cells (RBCs) were removed by addition of 5 mL DW into each sample tube softly, and each samples' hemoglobin solution was collected by centrifugation. The absorbance of the supernatants was measured by a multifunctional microplate reader (Infinite M200 Pro, Tecan) at 540 nm and record as A_s. 100 μL of citrated whole blood in 5 mL DW was utilized as the negative control, and its supernatants absorbance at 540 nm was recorded as A_n. The BCI was calculated using the following equation: (BCI (%) = (A_s/A_n) × 100%).

2.8.2. Coagulation time

270 μL CWB was mixed with 30 μL of 0.2 M calcium chloride ($CaCl_2$). Subsequently, the above mixture was blended with 3 mg of prewarmed samples. The time of the process from when the sample contacted the blood until the mixture completely ceased to flow was recorded.

2.8.3. Blood cells adhesion

According to previous reports, platelet-rich plasma (PRP) and concentrated RBCs were achieved by centrifugation [2,10]. For platelet adhesion, 100 μL of PRP were co-cultured with each sample for 30 min at 37 °C. Afterward, the adhered platelets were first fixed with 2.5% glutaraldehyde in PBS solution and counted by LDH kit after being gently washed with PBS three times, and 100 μL of PRP was used as the reference value. The percent of adhered platelets was counted using the following Eq: (platelet adhesion percentage (%) = (OD_{sample}/$OD_{reference\ value}$) × 100%). Moreover, the adhered platelets were also observed with SEM after fixation, a series of ethanol solution dehydration and drying.

As RBC's attachment, the concentrated RBCs were resuspended into PBS with the volume ratio of 1:1. 100 μL of the suspension was co-cultured with each sample for 30 min at 37 °C. And 100 μL of the suspension alone was used for the reference value. After that, the attached RBCs were lysed with 10 mL DW after being rinsed with PBS. Finally, 100 μL of lysed liquid was tested with a multifunctional microplate reader at 540 nm. The percent of adhered RBCs were counted using the following Eq: (RBC attachment percentage (%) = (OD_{Sample}/$OD_{Reference\ Value}$) × 100%). Furthermore, the RBC on the surface of each sample was also observed with SEM.

2.8.4. PRP coagulation

45 μL PRP was mixed with 45 μL PBS, HA or HA-ADP (final concentration 1w/v%) in 96 well-plate and warmed for 3 min, respectively. Then, 10 μL of 0.2 M calcium chloride ($CaCl_2$) was added. The coagulation time was tested with an UV–vis spectrometer at 405 nm. The coagulation time of platelet-poor plasm (PPP) was also tested by the same method.

Similarly with the whole blood coagulation test, 270 μL PRP was first mixed with 3 mg hydrogel sponge samples and warmed for 5 min. Afterward, 30 μL of 0.2 M calcium chloride ($CaCl_2$) was added and blended. The time of the process from when the sample contacted the blood until the mixture completely ceased to flow was recorded. Furthermore, prasugrel (final concentration 100 μM) treated PRP and PPP coagulation time were also accessed as the above producer.

2.8.5. In vivo hemostasis

36 SD (~300 g) rats were randomly assigned into 6 groups: control group, CELOX group, GS group, HA/CS group, HA/UCS group, and HA-ADP/UCS group. Before the evaluation, the rats were feed with sufficient water and food-forbidden for 12 h and were anesthetized with 3% (w/v) pentobarbital sodium by the intraperitoneal injection. Afterward, the rats were fixed on the operating bench and each rat's tail was cut off in the middle and untreated 30 s for free bleeding. Subsequently, the incision was treated with the test material and filter paper as a control group. The blood loss was collected by pre-weighed test materials or filter paper and the bleeding time was recorded by stopwatch.

Additionally, rat femoral artery injury was also evaluated. Briefly, the femoral artery was exposed with a scalpel and an injury was created by using an 18G needle. After that, each test material or filter paper was applied to the bleeding site. The blood loss amounts and hemostatic times in the animal experiments were recorded.

2.9. Wound healing

According to the former reports, full-thickness wound healing experiments were implemented with minor revision [5,10]. Four 10 mm round full-thickness skin defects were cut on the dorsal of Sprague-Dawley (SD) rats (weight of 200–250 g) under anesthetized and each wound was treated with the test materials. Meanwhile, a sterile gauze-treated wound was used as control (Fig. S1). After treatment of day 3, 7, and 14, the wound area tissue was collected and soaked in 4% paraformaldehyde solution after imaging for areas measurement by Image J. In addition, the pathological section of wound tissue was also stained by H & E, Masson, and immunohistochemistry and the images were captured by a scanner (Pannoramic DESK, 3D Histech, Hungary).

Immunohistochemical section was scanned by digital tissue section scanner and read by image analysis system (Wuhan Service-bio Technology Co. Ltd.). Positive grade was first performed: negative means no staining and counted as 0 point; light yellow is weakly positive, 1 point; brownish-yellow is medium positive, 2 points; tan is strongly positive, 3 points. The percent of positive area ratio was counted using the following Eq: (Positive area ratio (%) = (positive area/tissue area) × 100%) [27]. Histochemistry score (H-Score) is a histological scoring method by converting the positive number and staining intensity in each section into corresponding values to achieve semi-quantitative staining of tissues. H-Score was counted using the following Eq: (percentage of weak intensity area × 1) + (percentage of moderate-intensity area × 2) + (percentage of strong intensity area × 3). H-Score is a value between 0 and 300, and the larger the value is the stronger the comprehensive positive intensity is [28,29].

All the above-mentioned experimental animals, including the New Zealand White Rabbits and SD rats, were cared for and treated following the NIH guidelines for the care and use of laboratory animals (NIH Publication No. 85e23 Rev. 1985) as approved by the Research Center for Laboratory Animal of Shanghai Ninth People's Hospital, Shanghai Jiao Tong University School of Medicine.

2.10. Statistical

All data are expressed as mean ± standard deviation (SD) and analyzed using SPSS version 15.0 (SPSS, Inc., Chicago, IL, USA). One-way analysis of variance (ANOVA) and student t-test was used for the treatment comparison. Comparisons with *$p < 0.05$, **$p < 0.01$, ***$p < 0.001$, ****$p < 0.0001$ were considered statistically significant, the NS represented no significant difference.

3. Results and discussion

3.1. Hydrogel sponge characterization

Before the preparation of the HA-ADP/UCS hydrogel sponge, the

components of HA-ADP and UCS were first synthesized and characterized. As shown in Table S1 and Fig. S2A, various ADP-modified HA were prepared via the EDC/NHS coupling reaction and confirmed by observing the changes in the FTIR and ^{1}H NMR spectra. As shown in Fig. S2B, the FTIR spectrum of HA showed a broad peak at 3432 cm^{-1} that belongs to O–H stretching vibration, a mid-intensity peak at 1040 cm^{-1} that is assigned to the stretching vibration of C–O–C and C–O–H, and the peak at 2913 cm^{-1} that contributes to the C–H stretching vibration of the methyl or methine group of the hyaluronic acid molecule [30,31]. Also, from the FTIR spectrum of ADP, it was observed that there was a peak at 1275 cm^{-1} which corresponds to the symmetric stretching vibration of the P=O of the phosphate group, 880 cm^{-1} for P–O–P asymmetric stretching [31,32]. After ADP was conjugated to HA, both characteristic peaks of HA and ADP emerged in the FTIR spectrum of HA-ADP. Additionally, the appearance of the spectra at 1560 cm^{-1} and 1640 cm^{-1} corresponding to the amide II band and amide I band [30,32], respectively, confirmed that the amide bond was introduced onto the HA molecules. Moreover, the modification was confirmed by ^{1}H

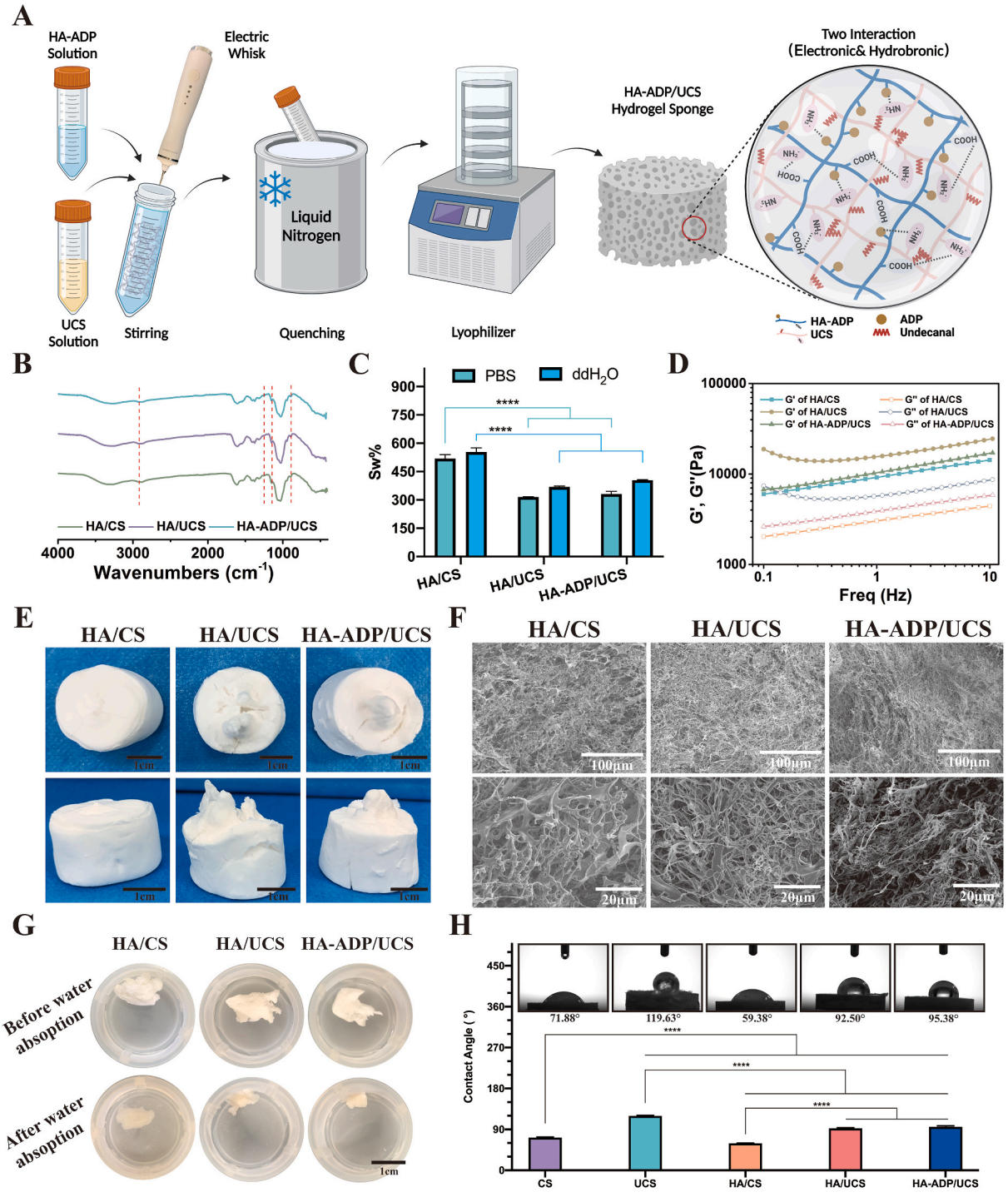

Fig. 1. HA-ADP/UCS preparation and its characterization. (A) Schematic illustration of HA-ADP/UCS hydrogel sponge preparation. (B) FTIR spectra of HA/CS, HA/UCS, HA-ADP/UCS. (C) The maximum water absorption ratio of all sponges. (D) Samples' rheological properties at the strain of 1%. (E) Samples' images after preparation. (F) SEM images of samples. (G) Samples' images before and after water absorption. (H) Contact angles of CS, UCS and as-prepared sponges. (*, $p < 0.05$; **, $p < 0.01$; ***, $p < 0.001$; ****, $p < 0.0001$).

NMR spectra, as indicated by the presence of new signals at around 2.79 ppm (Fig. S2C), which assigns to the amide bond formation that after ADP conjunction [4], and also the characterization signals of ADP at 8.33 and 8.56 ppm were also confirmed in ADP-modified HA [33]. These results confirmed the successful conjugation of ADP to HA. After that, the pro-coagulation performances of HA, various HA-ADPs, and PBS control for PRP were evaluated by testing the changes in optical density over time. As shown in Fig. S2D, HA-ADP groups showed a faster rise and plateau transition than the PBS control and HA groups. Additionally, HA-ADP30 and HA-ADP50 showed similar trend and were both faster than HA-ADP10. Based on the above results, HA-ADP30 was selected as the hydrogel sponge crosslink.

The UCS was prepared by covalently modifying CS with undecanal via sodium cyanoborohydride reduction (Table S2 and Fig. S3A). First, the antibacterial properties of the CS and UCS groups modified with different amounts of UDA were evaluated. As shown in Fig. S3D, there was almost no colony appearance in the ager plate after bacteria survivor re-suspending solution dropped on it in 10UCS. Due to the best antibacterial ability among the UCS groups, 10UCS was selected to synthesize the hydrogel sponge with HA-ADP. The UCS was also confirmed by FTIR and ^{1}H NMR. As shown in Fig. S3B, the FTIR peaks of CS were observed at 3450 cm $^{-1}$ (O–H) and 3360 cm $^{-1}$ (*N*–H) [34]. The peak at 1150 cm $^{-1}$ indicates the stretching vibration of the C–O single bond, and the peaks at 1070 cm $^{-1}$ and 890 cm $^{-1}$ correspond to C–O–C symmetric stretching vibrations [35]. After CS was conjugated with undecanal, the peak of UCS at 2900 cm^{-1} (–CH_2–) was enhanced and the appearance of the spectra at 1275 cm^{-1} corresponded to the stretching vibration peak of the C–N bond [2,36], indicating that CS and undecanal were chemically conjugated. Also, the ^{1}H NMR spectrum of CS and UCS was compared (Fig. S3C), it can be confirmed that the signals were observed at 0.74 ppm and 1.16 ppm in the ^{1}H NMR spectra of UCS, which contributes to the undecanal-tails. Additionally, because of the shielding of the signal of H-2 of the CS repeat-unit at 3.10 ppm, the signal of –CH_2 linked with N cannot be observed [25]. Moreover, the signal of methyl (-CH_3) as 1.95 ppm [37], which integral area compared to the H-2 of the CS repeat-unit at 3.10 ppm can reflects the changes of CS and UCS. The integral area ratio (-CH_3/H-2) were 0.18 and 0.24 for CS and UCS, which means the methyl increased after UDA's modification. All the above results demonstrate the successful conjugation of undecanal to CS.

After the successful synthesis of HA-ADP and UCS, HA-ADP/UCS was prepared by simply mixing a solution of 1% (w/v) HA-ADP and 1% (w/v) UCS at a volume ratio of 1:1 via vigorous stirring and electronic interaction crosslinking (Fig. 1A). Such a process is under the environmental friend condition that does not use any organic solvent or crosslinker. The as-prepared sponges were first confirmed by FTIR (Fig. 1B). It can be confirmed that all the samples showed the characteristic peaks of CS, UCS, HA, and HA-ADP, and there was no significant difference between groups, which could be attributed to the overlap of parts band vibration. In detail, the characteristic peaks of ADP at 880 cm^{-1} and 1275 cm^{-1} were overlapped with the peaks at 890 cm^{-1}(C–O–C) of CS and 1275 cm^{-1}(C–N) of UCS. The characteristic peaks of UCS at 2900 cm^{-1} (–CH_2–) was overlapped with the peak of HA at 2913 cm^{-1} for the C–H stretching vibration of the methyl or methine group of the hyaluronic acid molecule. Additionally, the contact angle test showed that the HA/UCS and HA-ADP/UCS exhibited more hydrophobic properties than HA/CS, which can relate to the components of UCS that display hydrophobic performance due to the conjugation of UDA (Fig. 1H). All the above results demonstrate the successful synthesis of the samples.

After that, the rheological properties of all samples were assessed. The results showed that the storage modulus (G′) and loss modulus (G″) of the hydrogels with different group conjugation as a function of frequency (Fig. 1D). In detail, the G′ and G″ of HA/UCS was higher than that of the other two groups, however, the G′ and G″ of HA- ADP/UCS decreased after ADP introduction. All of these changes could be attributed to the following aspects: the enhancement of G′ and G″ for HA/UCS and HA-ADP/UCS could be associated with the substitution of the amine group of CS and the carboxylic acid of HA, which could enhance the hydrophobic interaction between UDA groups of UCS (Fig. 1H) [36] and alter the density of electronic interactions between the amine group of CS and the carboxylic acid and diphosphate groups [14,38]. In addition, there were displayed clear potential changes before and after the modification of CS and HA (Fig. S4). Because the modification process of HA-ADP was replacing one carboxylic acid with two negatively charged phosphate groups, the number of charged groups changes could cause the enhancement of G′ and G″ for HA-ADP/UCS lower than that for HA/UCS. The morphologies of the samples were examined. As shown in Fig. 1E, the images of the samples displayed a bulk state, which is suitable as a dressing for forming a physical barrier for application to the bleeding site or wounded area. Additionally, the SEM images revealed that each sample exhibited a three-dimensional network structure and porous structure that made interstitial fluid and blood more readily absorbed, which contributed to hemostasis (Fig. 1F).

Effective fluid absorption from blood is a fundamental ability for a hemostatic material that promotes erythrocytes, fibrinogen, endogenous coagulation factors, and platelet concentration at the wound site [1,2]. As shown in Fig. S5, all samples presented the faster water absorption and achieved equilibrium water absorption after 8 min. Thus, the equilibrium water absorption capacity of the samples was evaluated after 10 min of soaking in DW and PBS (Fig. 1C and G). HA/CS can absorb 553.9% of water within 10 min of its initial weight. Comparably, the maximum water absorption of HA/UCS (368.54%) and HA-ADP/UCS (404.25%) were lower than those of HA/CS (553.94%), which could be related to the hydrophobic group of UCS. Moreover, the absorption of PBS has similar trends to that of DW. The images before and after water absorption of the samples showed that all the sample volumes were reduced and transformed their states from bulk to gel, which could promote blood cells adhering to the materials and shorten the distance between cells to aggregate. All the above results revealed that the as-prepared samples exhibited good water absorption, which is related to the following aspects: the inherent hydrophilic ability of HA can induce rapid water absorption, and it may also be induced by the various 3D porous microstructures [2]. Thus, the water absorption of the samples could determine the blood component concentration which can contribute to rapid hemostasis.

3.2. Cytocompatibility, hemolysis, and in vitro/vivo degradation

Biocompatibility is an essential requirement for hemostatic materials that can promote wound healing. Thus, the effects of the samples on cells were investigated via CCK8 and live/dead staining assays by using HUVEC and REPC as models. As presented in Fig. 2A and C, all cells exhibited a proliferation rate similar to that of the control group after co-culture with sample' DMEM extract for 1, 4, and 7 days, and the viability of cells was greater than 85%. Additionally, the direct contact between cells and samples was also confirmed by using the live/dead assays (Fig. 2B and D). The results in all groups showed that the cells' fluorescence was mostly green with normal morphology and very little red, indicating that all cells were alive. These results suggest that the as-prepared samples could favor cell adhesion and proliferation, which can support wound healing after hemostasis.

Inducing no or minimal hemolytic activity is an essential prerequisite for hemostatic material because of its direct contact with blood [39,40]. Thus, erythrocyte compatibility was determined by using the hemolysis ratio. The hemolysis ratios of all samples were lower than 5% (a considerable maximum level of acceptable hemocompatibility) (Fig. 2E), indicating that the as-prepared samples showed insignificant hemolytic activity. The pictures of hemoglobin released from erythrocytes also revealed the low hemolytic activity of the hydrogel sponges (Fig. 2F). All the above results showed that the samples had high blood compatibility.

Wound healing includes hemostasis, inflammation, proliferation,

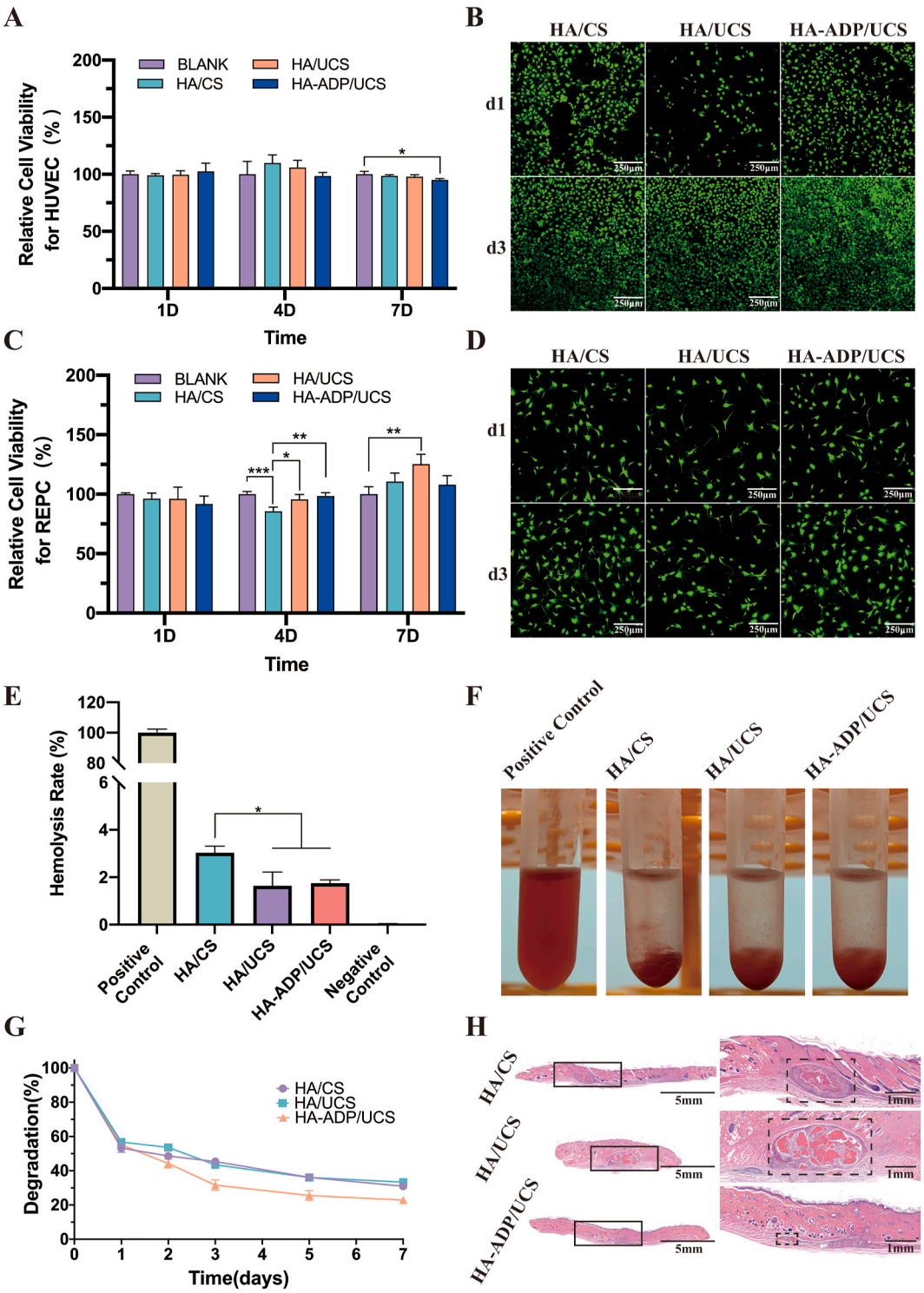

Fig. 2. Cytocompatibility and hemolysis test of HA/CS, HA/UCS, and HA-ADP/UCS. (A & B) Cell viability and confocal microscopy for HUVEC of control, HA/CA, HA/UCS, and HA-ADP/UCS. (C & D) Cell viability and confocal microscopy for REPC of control, HA/CA, HA/UCS, and HA-ADP/UCS. (E) Hemolysis assays of HA/CS, HA/UCS, and HA-ADP/UCS. (F) Images after hemolysis. (G) Degradation curve of HA/CS, HA/UCS and HA-ADP/UCS *in vitro*. (H) H & E staining of HA/CS, HA/UCS and HA-ADP/UCS after 30 days *in vivo*. (*, $p < 0.05$; **, $p < 0.01$; ***, $p < 0.001$).

and remodeling stages [41]. To promote wound healing, the as-prepared samples should not only exhibit excellent biocompatibility but also be biodegradable for the regeneration of new tissues. As shown in Fig. 2G and H, the weight of all samples was gradually lost *in vitro*. The weight loss of HA/CS, HA/UCS, and HA-ADP/UCS were 69.05%, 66.67% and 77.22%, respectively, after 7 days *in vitro*. In particular, the degradation of HA-ADP/UCS was faster than that of HA/CS. The variation in degradation between the groups could be attributed to the changes in electronic interaction [14]. The modification of HA and CS can transfer the carboxyl and amino groups into an amide carbon-nitrogen bond, which changes the electrical properties of these groups and forms hydrophobic interactions. The changes in the samples *in vivo* were also evaluated via histological staining assay for the experimental tissue sites after the set time of implantation. It revealed that sample residues that

were stained purple-brown could be visible on the majority of sections after implantation for 10 days (Fig. S6). Additionally, all samples presented a few infiltration of inflammatory cells, with a mass of fibroblasts around the samples. After implantation for 30 days, the experimental tissue sites of HA-ADP/UCS were not only without the residual fragments of the remaining samples but also did not have an evident pathological response. However, there still existed a few residual fragments of HA/CS and HA/UCS; the number of inflammatory cells and fibroblasts around them was decreased compared with before 10 days and 20 days (Fig. S6). These results illustrate that the HA-ADP/UCS samples exhibited excellent degradability.

3.3. *In vitro and in vivo hemostatic performance*

To test the samples' pro-coagulation performance, the blood clot index (BCI) was first tested. The absorbance value of the uncoagulated RBCs' hemoglobin solution was employed to assess BCI, in which a minor value of BCI indicates rapid pro-coagulation ability [39]. As shown in Fig. 3A and C, the BCI values of all samples were lower than those of the blank control, indicating the excellent pro-coagulation performance of the as-prepared samples. However, there was no significant difference between the groups, which could be related to incomplete contact between the sample and blood due to the hydrophobic modification of CS. Moreover, the blood clotting time (BCT) was assessed *in vitro* (Fig. 3B and D). The BCT of whole blood without any treatment to completely coagulate was transformed to 100%. Comparably, the BCT of HA/CS, HA/UCS, and HA-ADP/UCS were reduced to 97.81%, 96.40% and 58.94%, respectively. All the above results indicate that the as-prepared HA-ADP/UCS sample exhibits excellent pro-coagulation performance.

Blood cell aggregation is an important factor in the primary hemostasis stage [42,43]. CS and hm-CS can form an electronic interaction or hydrophobic interaction with the negatively charged membranes of blood cells, thereby inducing blood cell aggregation [14,21,23]. Thus, the RBC and platelet adhesion were first assessed, which revealed that all the samples performed excellent adhesion to RBCs and platelets. In particular, the quantified RBC and platelet adhesion in Fig. 4E and G showed that HA-ADP/UCS had the highest number of cell attachments compared to the other two groups. The morphologies of RBC and platelets on each sample were also observed by using SEM, and the results showed that RBC on HA/UCS and HA-ADP/UCS changed to an irregular and angular shape that was significantly different from RBC on HA/CS (Fig. 4F), and abundant platelet aggregates and more substantial platelet pseudopod formation were observed on HA-ADP/UCS compared to other groups (Fig. 4H). All those results could refer to the following respects: the protonated CS's amine groups can form an electrostatic interaction with the negatively-charged blood cell membranes and also UDA modified CS residues can anchor the hydrophobes of UCS into the hydrophobic interiors of blood cell membranes [2,25], causing strong hemagglutination.

Blood cell activation is another crucial element for cell plug formation in primary hemostasis [42], especially for platelet activation in the

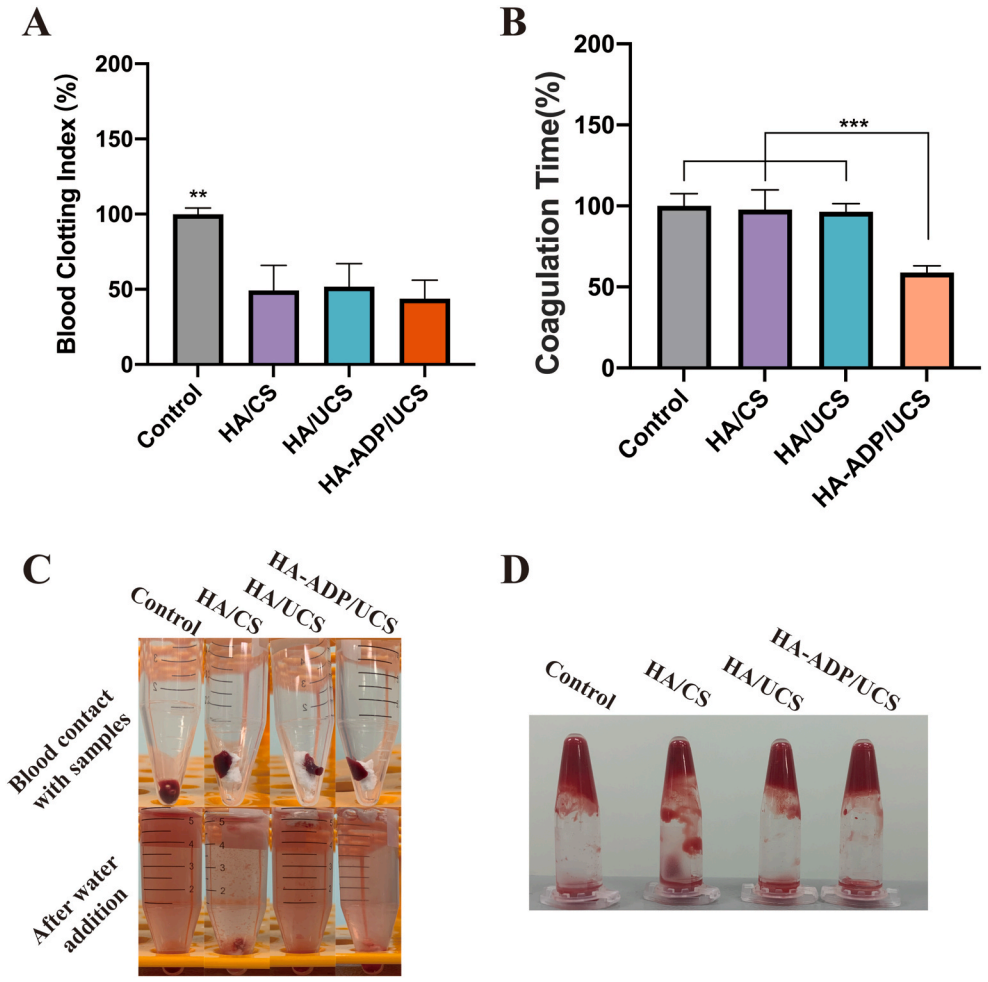

Fig. 3. The pro-coagulation performance of samples. (A) Blood clotting index of control, HA/CS, HA/UCS, and HA-ADP/UCS. (B)Whole blood coagulation time of control and test samples. (C)The images of samples before and after the BCI test. (D) The images of samples after whole blood coagulation. (**, $p < 0.001$; ***, $p < 0.001$).

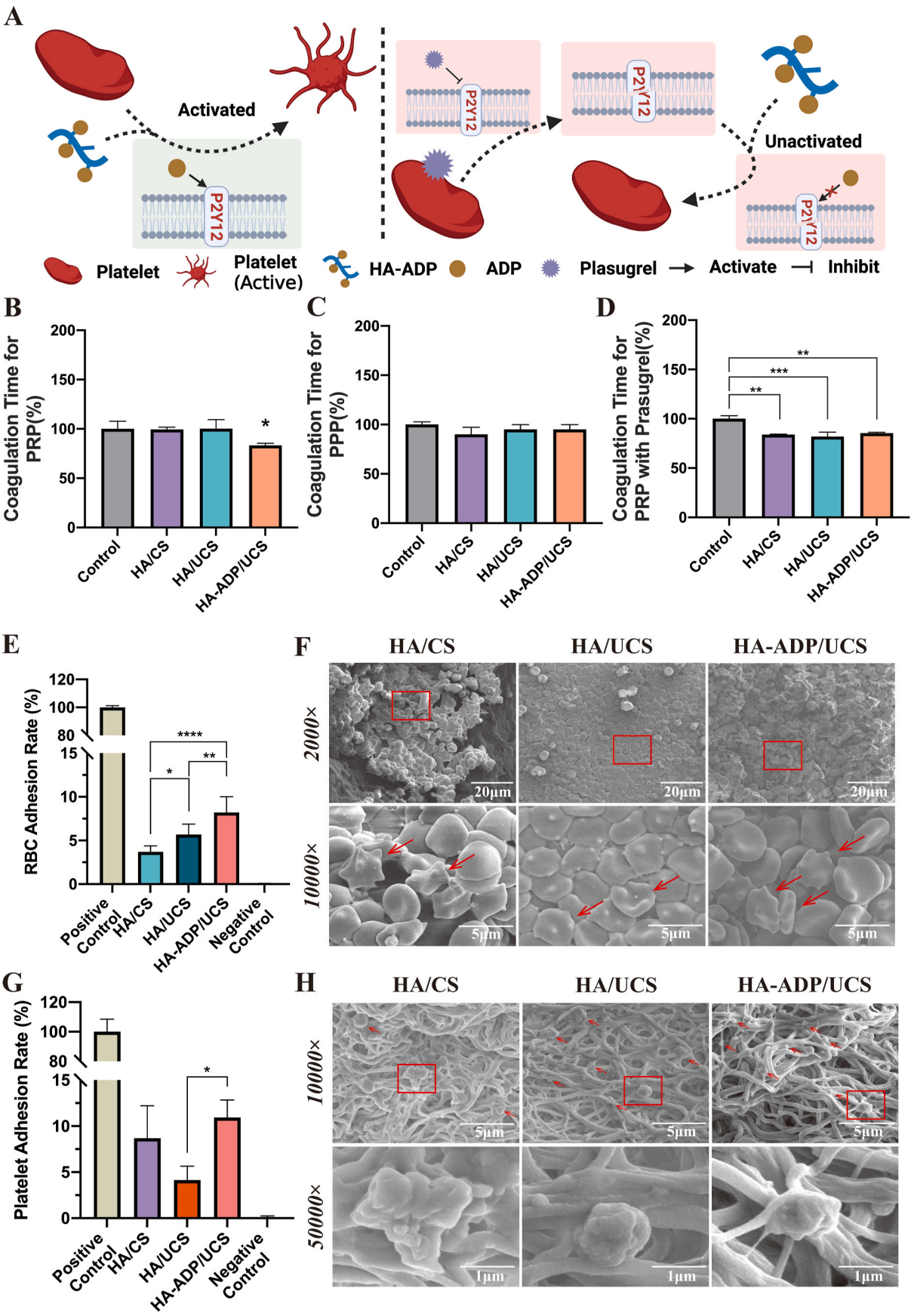

Fig. 4. Blood cells adhesion characterization. (A) Schematic illustration of HA-ADP activates platelet mechanism. (B) Coagulation time of PRP treated with different samples. (C) Coagulation time of PPP. (D) Coagulation time of PRP pretreated with prasugrel. (E&G) RBC and platelet adhesion rate of control and samples. (F&H) Morphologies of RBC and platelet adhered to different samples by SEM. (*, $p < 0.05$; **, $p < 0.01$; ***, $p < 0.001$; ****, $p < 0.0001$).

spontaneous primary stage of hemostasis. The previous hypothesis was that the ADP-modified HA posed the same potential to activate platelets to promote platelet dense granule formation and accelerate hemostasis. Thus, the influence of the as-prepared samples on PRP coagulation time was assessed. The results showed that HA-ADP/UCS had the shortest time compared to HA/CS and HA/UCS (Fig. 4B). Moreover, the PPP coagulation time was assessed. Comparably, the samples treated groups possessed a shorter time than that of the blank control, and there was no significant difference between the groups (Fig. 4C). Also, the coagulation time of prasugrel, an irreversible inhibitor for the G protein-coupled receptor of P2Y12 that can bind with ADP to active platelet [19], treated PRP was also tested. It can be confirmed that HA-ADP/UCS coagulation time has almost no shorter time than that of HA/CS and HA/UCS (Fig. 4D). Additionally, the pro-coagulation performances of HA and HA-ADP for PRP and PPP were evaluated by testing the optical density changes with time. HA-ADP showed a faster rise and plateau transition than the PBS control and HA groups in the PRP test (Fig. S1D), and this trend was not observed in the PPP test (Fig. S7). All the above results revealed that ADP-modified HA can activate platelets via the P2Y12 receptor, which accelerates hemostasis (Fig. 4A). Meanwhile, the negatively charged group of HA or HA-ADP specifically activated the contact pathway that facilitates the coagulation cascade, which could provide positive feedback support for promoting coagulation.

Based on the *in vitro* hemostasis performance, the hemostasis capability of the as-prepared samples in a real wound was also assessed through rat-tail amputation and rat femoral artery injury model, CELOX, and gelatin sponge (GS) were used as controls. For rat-tail amputation, half of the rat tail was cut and treated with various samples (Fig. 5A).

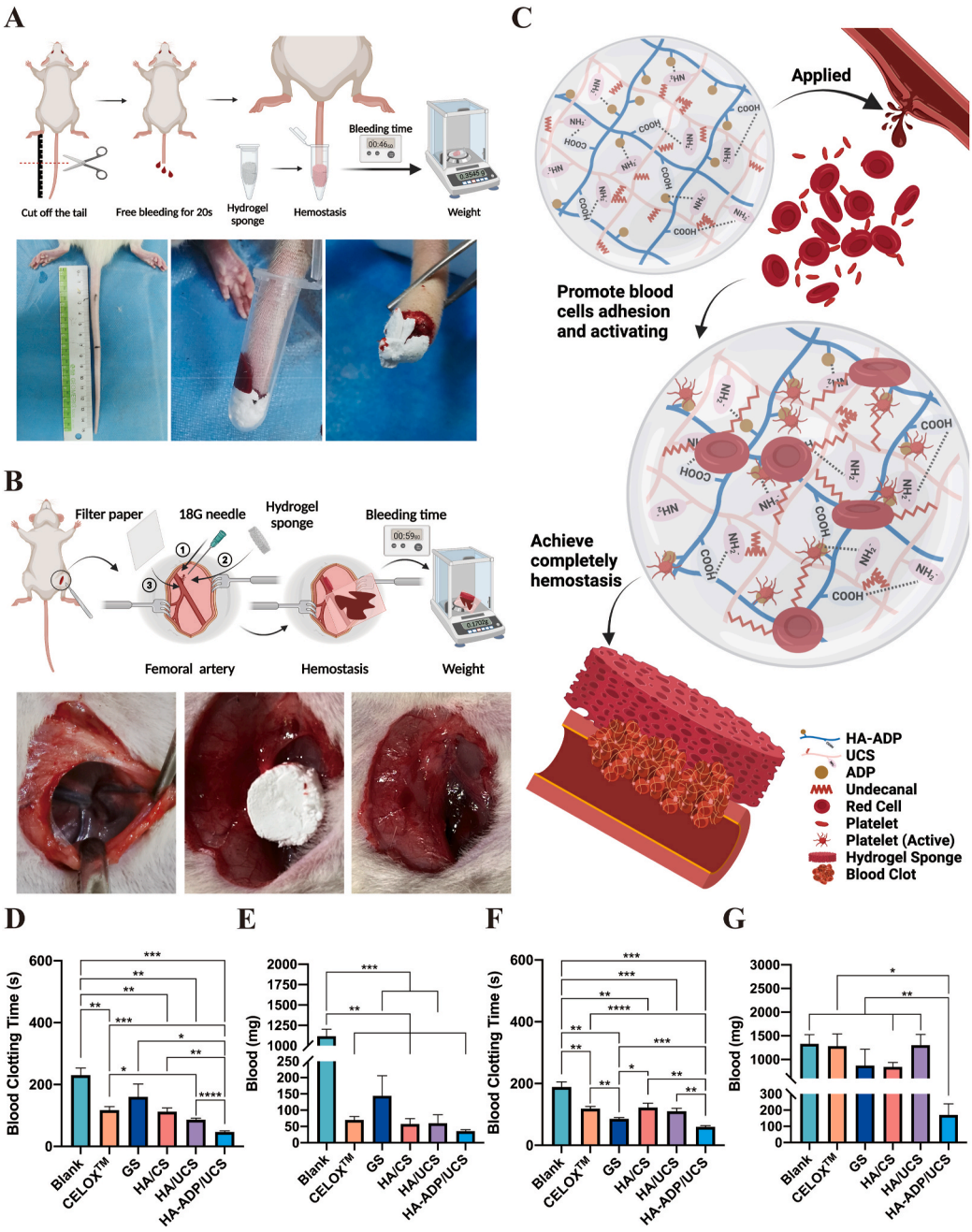

Fig. 5. *In vivo* hemostasis performance of samples. (A) Schematic illustration and images of rat-tail amputation hemostasis model. (B) Schematic illustration and images of rat artery injury hemostasis model. (C) Schematic illustration of HA-ADP/UCS internal hemostasis process. (D & E) Hemostasis time and blood loss from bleeding rat tails. (F & G) Hemostasis time and blood loss from rat bleeding arteries. (*, $p < 0.05$; **, $p < 0.01$; ***, $p < 0.001$; ****, $p < 0.0001$).

The results of hemostatic time and blood loss showed that the HA-ADP/UCS group not only had the shortest hemostatic time but also possessed minimum blood loss, which is also superior to that of the commercially available CELOX and GS (Fig. 5D and E). In particular, the hemostatic time was shortened from 230 s in the blank group to 112 s in HA/CS, 86 s in HA/UCS and 46 s in HA-ADP/UCS; and the blood loss decreased from 1116 mg in the blank group to 57 mg in HA/CS, 59 mg in HA/UCS and 35 mg in HA-ADP/UCA, respectively. The effects of various samples on blood clotting time and blood loss weight were also evaluated in the femoral artery injury experiment (Fig. 5 B, F, G, and Movie S1).

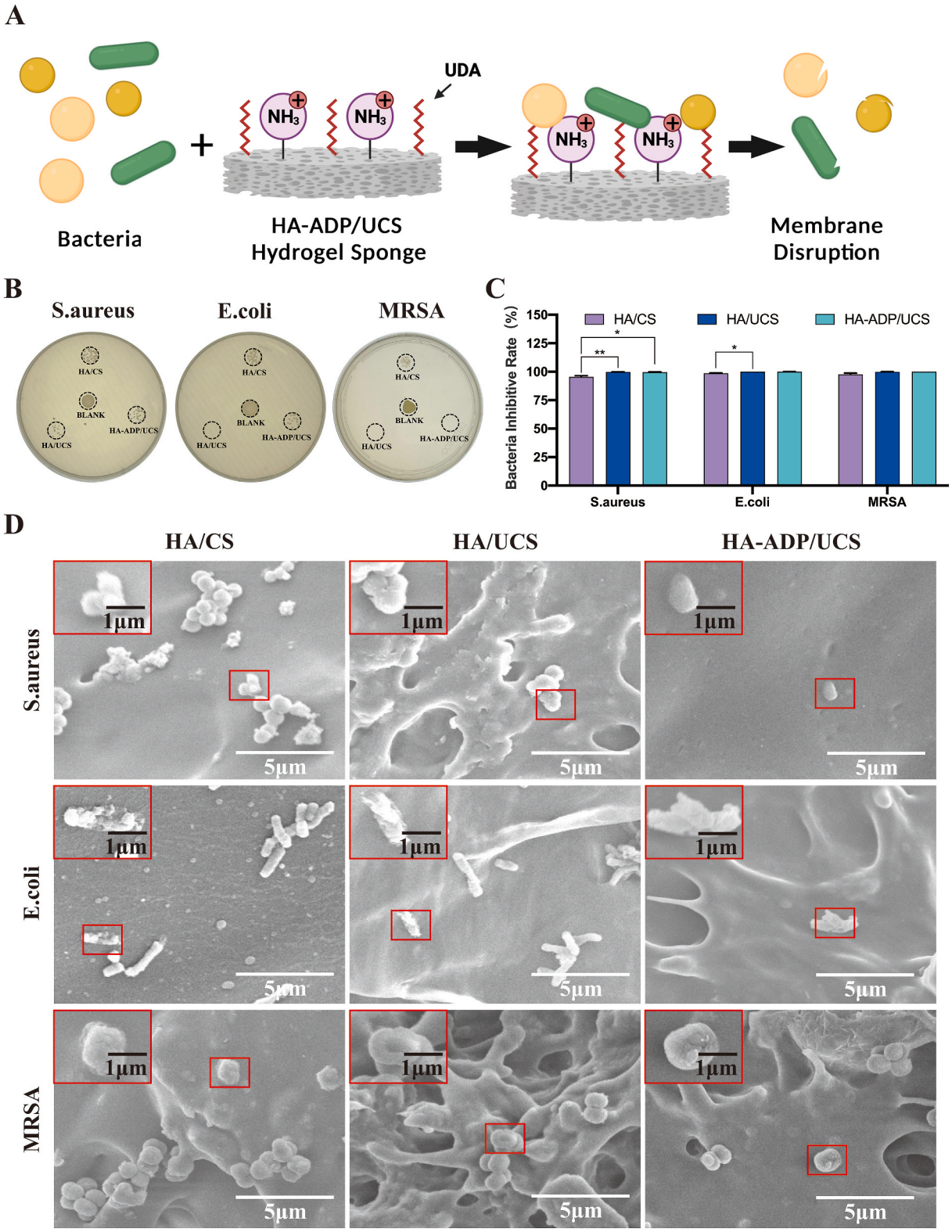

Fig. 6. *In vivo* antibacterial performance of samples. (A) Schematic illustration of antibacterial property of HA-ADP/UCS hydrogel sponge. (B) Bacteria survivor resuspending solution dropped on agar plate after 24 h. (C) Statistical results of antibacterial properties. (D) Morphologies of bacteria on samples surface by SEM (10000 × and 20000 ×). (*, $p < 0.05$; **, $p < 0.01$).

Comparably, the as-prepared HA-ADP/UCS took the shortest time to complete cessation of bleeding (59 s) and led to the least blood loss (170 mg), which was also better than that of commercial CELOX, GS and other samples. These results suggest that HA-ADP/UCS has the superior pro-coagulation ability both *in vitro* and *in vivo*.

The mechanism of the hemostatic performance of the sponges is related to their unique physicochemical properties. The bulk state of the materials can prevent blood loss from the wounded area by forming a physical barrier, and the porous structure of the materials provides high surface area and large volume for wound exudes absorbance and blood component adhesion. The wound exudes absorbance can extract fluid in the blood that concentrates blood cells, proteins, and other active ingredients [44], simultaneously, these components could adhere to the surface of the materials and reinforce them through electrostatic and hydrophobic interactions. Meanwhile, the functional group of the material can activate the adhered platelets and promote coagulation cascades that facilitate the coagulation system in both extrinsic and intrinsic pathways, which eventually contribute to its prominent hemostatic properties (Fig. 5C).

3.4. Antibacterial properties

Wound infection easily occurs in a dirty environment after severe bleeding, which can hinder the physiological healing process and even lead to life-threatening complications. Thus, an ideal hemostatic material should have antibacterial properties during its application. CS and its hydrophobic derivatives possess excellent antibacterial capabilities [23,24]. To assess the antibacterial efficacy, the as-prepared samples were utilized for separate co-cultures with gram-positive *S. aureus*, gram-negative *E. coli*, and MRSA. As shown in Fig. 6B, there was almost no colony appearance in the ager plate after bacteria survivor re-suspending solution dropped on it, indicating that more than 95.49% of *S. aureus*, *E. coli* and MRSA on the surface of the hydrogel sponge were killed (Fig. 6C). The antibacterial ability of HA/CS, HA/UCS, and HA-ADP/UCS were 95.49%, 99.74%, 99.55% for *S. aureus*, 98.63%, 100.00%, and 99.97% for *E. coli*, and 97.65%, 99.89%, and 100.00% for MRSA. The results indicate that the antibacterial properties of HA/UCS and HA-ADP/UCS were better than those of HA/CS, and the enhanced antibacterial performance was mainly attributed to UCS, which had an excellent bactericidal effect compared to CS, HA, and HA-ADP (Fig. S3D and Fig. S8). Meanwhile, all three bacteria lost their physiological structure after contacting the surface of the samples (Fig. 6D), which revealed that the sample could destroy the cell membranes and lead to the nucleic acid inside to outflow and accumulation of nucleic acids (Fig. 6A) [23]. The excellent antibacterial properties of the samples could be related to the bacterial disruption abilities of CS and UCS.

3.5. Wound healing

In addition to hemostasis, wound healing is another problem to be addressed. Therefore, the samples were employed as the test group to assess the efficacy of treatment for infected wounds and using standard gauze as a control group. As shown in Fig. 7A and B, the wound area progressively narrowed, and the wound closure rate increased gradually with time. In particular, the hydrogel group showed a smaller wound area and higher wound closure rate on day 3 than the gauze group. With time, all groups' close rates were significantly increased on day 7, and the HA-ADP/UCS group presented the best effect that surpassed approximately 20% compared to the control group. The wound healing differences among the groups gradually decreased, and eventually, all the defects were almost completely healed on day 14, which was consistent with reported wound healing experiments [45,46]. The results demonstrated that the HA-ADP/UCS group exhibited excellent properties in accelerating wound closure. For further observation of wound healing, histomorphology analysis of the regenerative skin tissue was also conducted to evaluate the therapeutic efficacy of the samples during the healing phases (Fig. 7C and D). On day 3 of treatment, each group presented an obvious defect in the epidermal and dermal structures of the skin. There was little or no collagen filling in the skin defect. Simultaneously, the test groups showed less infiltration of inflammatory cells than the control group. On day 7 of treatment, an immature, thicker epithelium was observed in the test group. Meanwhile, collagen gradually increased in the defect site, especially in the HA-ADP/UCS group. After 14 days of treatment, each group showed complete epithelial and dermal structures, with the HA-ADP/UCS groups presenting the thinnest epidermis and the largest amount of newly formed blood vessels as well as hair follicles, which is the most normal tissue-like structure of remodeled tissue. Collagen filling was also observed in all the groups.

The short length of polyphosphate-modified material can induce milder acute inflammation in the early stage of wound healing [31]. ADP is a derivative of polyphosphate that has two repeat phosphate units, which could also have the ability to adjust the wound site inflammation. Thus, the inflammatory effects of the samples were evaluated. The typical proinflammatory cytokines of IL6 in the early healing stage were characterized both *in vitro* and *in vivo*. As shown in Fig. 8B, HA-ADP/CUS exhibited higher IL-6 expression than HA/CS and HA/UCS *in vitro* test co-cultured with REPC for 3 days. In addition, immunohistochemistry staining of these samples showed the same results on day 3 (Fig. 8 A, C and D). To further observe the role of IL-6 in wound healing, the same tests *in vivo* were repeated on day 7 and day 14. As shown in Fig. 8 A, C and D, the positive areas of all groups were increased at day 7 and decreased at day 14, and the H-score continued to decrease. Moreover, the changes in each group during the wound period were compared (Fig. S9), in which the HA-ADP/UCS showed a similar trend as the uninfected group, while the IL-6 expression of HA/CS and HA/UCS increased on day 7 and remained almost unchanged thereafter. IL-6 has been reported to improve vascularization and collagen deposition, which can accelerate the wound healing process [47]. However, prolonged stimulation of IL-6 affects non-healing wounds or fibrosis, because the inflammation phase cannot shift to the anti-inflammatory phase [48]. The upregulation of IL-6 in the HA-ADP/UCS group at day 3 could decrease the inflammation phase and accelerate the wound healing process. After that, the timely descent of IL-6 at day 7 and 14 could prevent the inhibition of wound healing by long-term IL-6 action. Additionally, there were no significant differences between the control and test groups in TNF-α expression *in vivo* (Fig. S10) and no obvious TNF-α expression was observed in all groups *in vitro*. All the above results demonstrated that HA-ADP/UCS could promote the expression of IL6, which could shorten the wound healing time via inflammation adjustment [49].

The excellent wound healing properties of the as-prepared samples could be attributed to the following reasons: the hydrogel sponges had the superior hemostatic characteristic of decreasing blood loss by promoting the defect from forming a physical barrier and maintaining a moist microenvironment; additionally, the hydrophobic alkyl group modified CS impedes bacterial infection; and ADP modified HA can promote the phagocytosis of inflammatory cells and regulate the inflammatory response in the early healing phase, which can speed up the transition from the hemostasis/inflammation phase to the proliferation phase, and thus induce rapid wound healing. Moreover, the excellent cytocompatibility of the samples can promote cell migration and proliferation, which also promotes skin tissue remodeling.

4. Conclusion

A bioinspired and biodegradable HA-ADP/UCS hydrogel sponge was successfully designed and crosslinked through electronic interactions. The as-prepared hydrogel sponge has an excellent porous structure and a great ability for water absorption, which can be influenced by the hydrophobicity of UCS. Moreover, all samples exhibited biocompatibility, biodegradability, antibacterial performance, and negligible hemolysis. Additionally, HA-ADP/UCS exhibited a considerable hemostatic

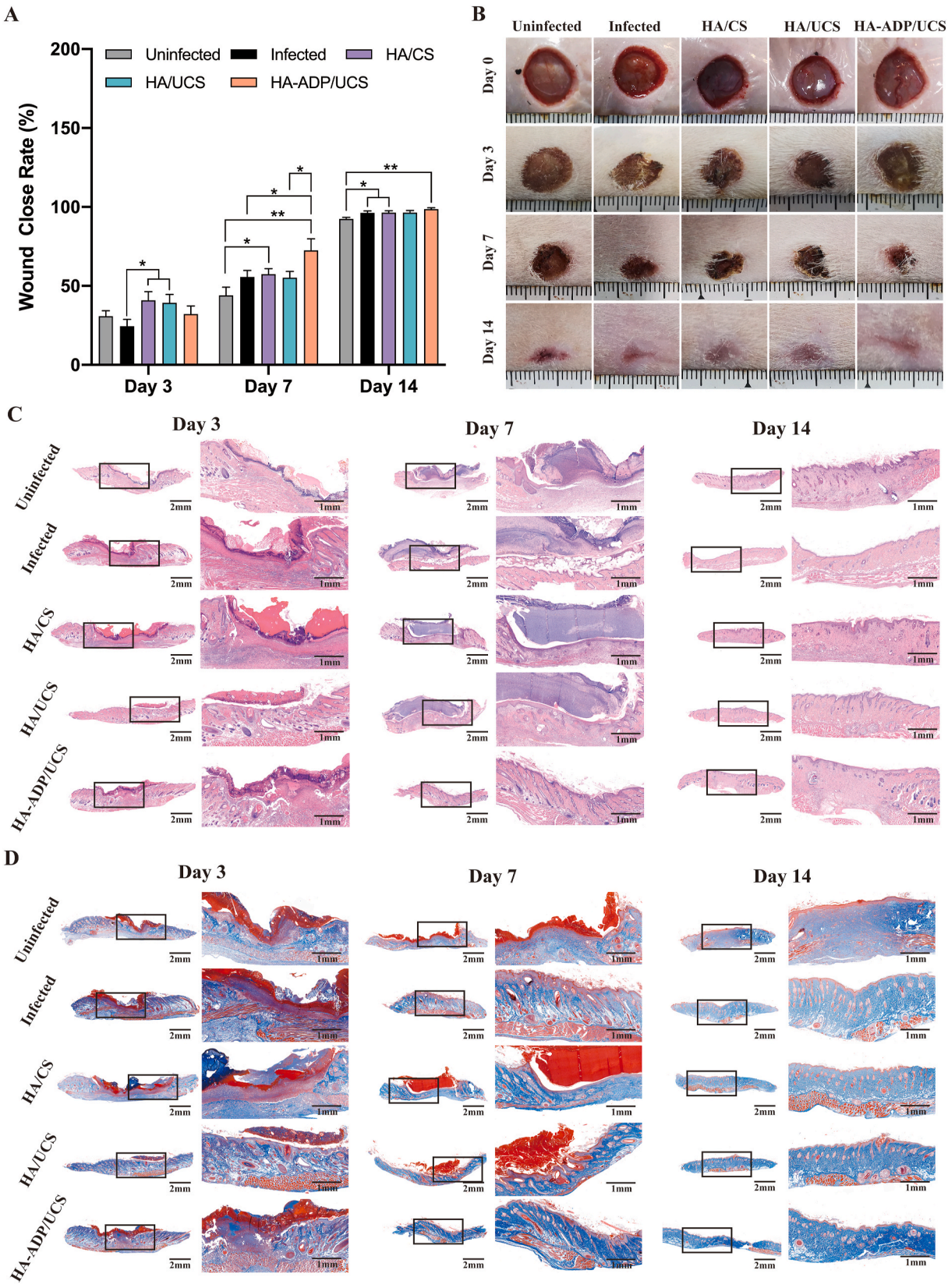

Fig. 7. Wound healing performance of the samples. (A) Wound close rate of the samples at set time points. (B) Wound images of various samples. (C&D) Histomorphology evaluation of wound regeneration at set time points, H&E staining, and Masson staining. (*, $p < 0.05$; **, $p < 0.01$).

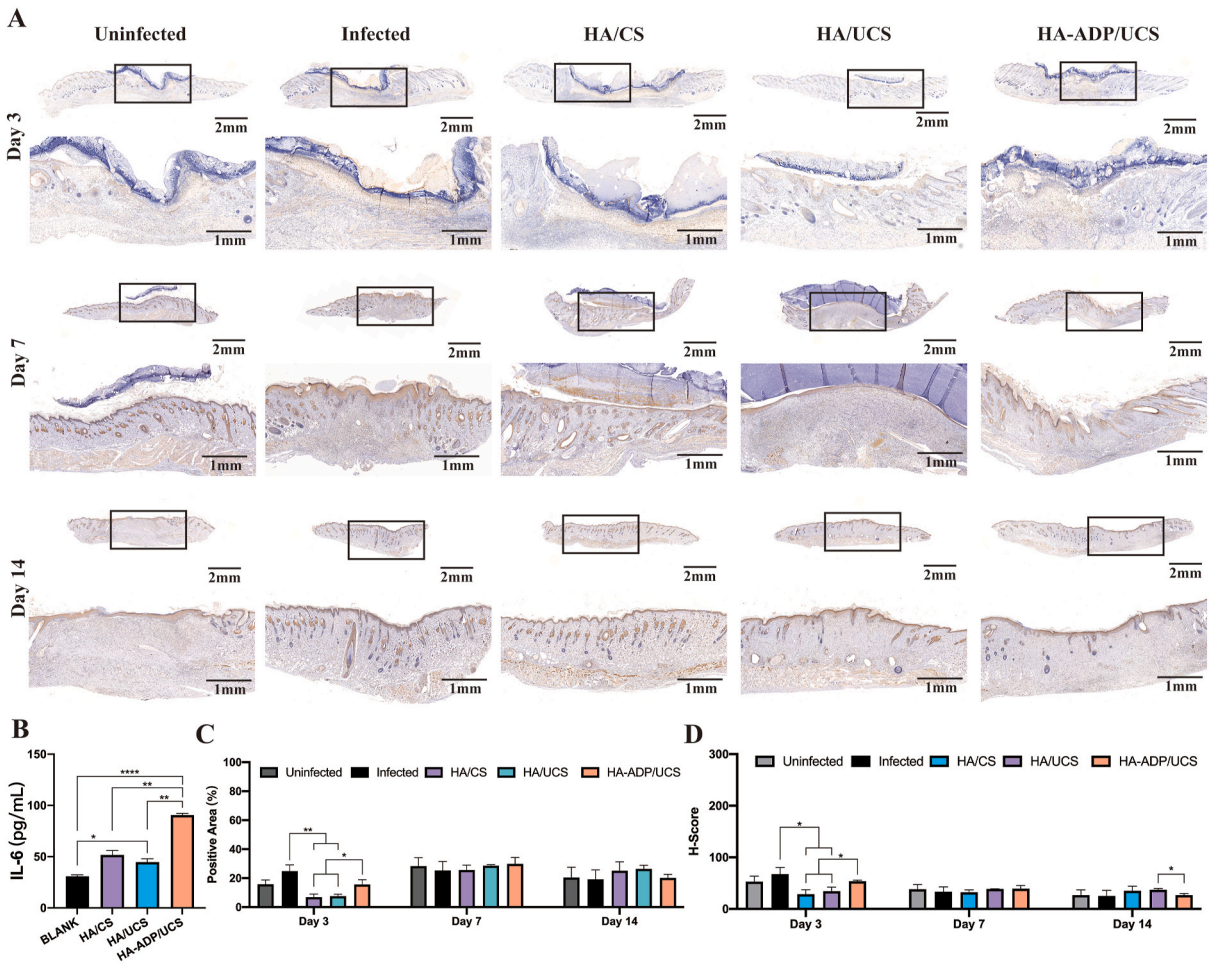

Fig. 8. Immunohistochemistry and ELISA of samples. (A) IL-6 Immunohistochemistry staining of various samples at day 3, 7, and 14, positive areas are brown. (B) IL-6 level at day 3 of each sample evaluated by ELISA *in vitro*. (C) Positive area ratio at day 3, 7, and 14 for IL-6. (D) Histochemistry score at day 3, 7, and 14 for IL-6. (*, $p < 0.05$; **, $p < 0.01$; ***, $p < 0.001$; ****, $p < 0.0001$)

performance via electrostatic and hydrophobic interactions, and water absorption to enhance blood component concentration and facilitate adhesion of these components; in particular, the adhered platelets can be activated by HA-ADP. In addition, HA-ADP/UCS possesses a superior hemostasis ability compared to commercially available CELOX and GS. Furthermore, HA-ADP/UCS can also promote the wound healing process due to its biocompatibility, biodegradability, hemostatic, and antibacterial effects to achieve rapid hemostasis, sterilize wound sites, and adjust wound inflammation reaction to provide a suitable microenvironment. We are convinced that HA-ADP/UCS would provide clinical hemorrhage mastery with an effective approach and has the potential for a commercial large-scale production application.

CRediT authorship contribution statement

Yihao Liu: Conceptualization, Methodology, Validation, Formal analysis, Investigation, Writing – original draft, Writing – review & editing, Visualization. **Haoyi Niu:** Conceptualization, Methodology, Formal analysis, Writing – review & editing. **Chengwei Wang:** Conceptualization, Methodology, Validation, Formal analysis, Investigation, Writing – original draft, Writing – review & editing, Visualization, Funding acquisition. **Xiaoxiao Yang:** Formal analysis, Writing – original draft, Visualization. **Wentao Li:** Methodology, Writing – original draft, Visualization. **Yuxin Zhang:** Formal analysis, Writing – review & editing, Visualization. **Xiaojun Ma:** Writing – review & editing, Visualization. **Yuanjing Xu:** Writing – review & editing, Visualization. **Pengfei Zheng:** Conceptualization, Methodology, Validation, Investigation, Writing – review & editing, Supervision, Funding acquisition. **Jinwu Wang:** Conceptualization, Methodology, Validation, Investigation, Writing – original draft, Writing – review & editing, Supervision, Project administration, Funding acquisition. **Kerong Dai:** Conceptualization, Methodology, Validation, Investigation, Writing – review & editing, Visualization, Supervision, Funding acquisition.

Declaration of competing interest

The authors declare that they have no known competing financial interests or personal relationships that could have appeared to influence the work reported in this paper.

Acknowledgments

Figs. 1A, 4A and 5 A&B&C, 6A and S1 were created with BioRender.com.

The study was supported by the National Key R&D Program of China (2018YFA0703000), China Postdoctoral Science Foundation (2020M681320), National Nature Science Foundation of China (grant nos. 82072969) Jiangsu Provincial Key Research and Development Program (CN) (BE2019608), National Natural Science Foundation of China (82072412/81772326) and Project of Shanghai Science and Technology Commission (19XD1434200/18431903700).

Appendix A. Supplementary data

Supplementary data to this article can be found online at https://doi.org/10.1016/j.bioactmat.2022.01.025.

References

[1] X. Yang, M. Chen, P. Li, Z. Ji, M. Wang, Y. Feng, C. Shi, Fabricating poly(vinyl alcohol)/gelatin composite sponges with high absorbency and water-triggered expansion for noncompressible hemorrhage and wound healing, J. Mater. Chem. B 9 (6) (2021) 1568–1582, https://doi.org/10.1039/d0tb02480e.

[2] X. Wei, S. Ding, S. Liu, K. Yang, J. Cai, F. Li, C. Wang, S. Lin, F. Tian, Polysaccharides-modified chitosan as improved and rapid hemostasis foam sponges, Carbohydr. Polym. 264 (2021), 118028, https://doi.org/10.1016/j.carbpol.2021.118028.

[3] R. Hao, X. Peng, Y. Zhang, J. Chen, T. Wang, W. Wang, Y. Zhao, X. Fan, C. Chen, H. Xu, Rapid hemostasis resulting from the synergism of self-assembling short peptide and O-carboxymethyl chitosan, ACS Appl. Mater. Interfaces 12 (50) (2020) 55574–55583, https://doi.org/10.1021/acsami.0c15480.

[4] W. Huang, S. Cheng, X. Wang, Y. Zhang, L. Chen, L. Zhang, Noncompressible hemostasis and bone regeneration induced by an absorbable bioadhesive self-healing hydrogel, Adv. Funct. Mater. 31 (22) (2021), https://doi.org/10.1002/adfm.202009189.

[5] H. Yuan, L. Chen, F.F. Hong, A biodegradable antibacterial nanocomposite based on oxidized bacterial nanocellulose for rapid hemostasis and wound healing, ACS Appl. Mater. Interfaces 12 (3) (2020) 3382–3392, https://doi.org/10.1021/acsami.9b17732.

[6] D. Wang, W. Li, Y. Wang, H. Yin, Y. Ding, J. Ji, B. Wang, S. Hao, Fabrication of an expandable keratin sponge for improved hemostasis in a penetrating trauma, Colloids Surf. B Biointerfaces 182 (2019), 110367, https://doi.org/10.1016/j.colsurfb.2019.110367.

[7] M. Long, Y. Zhang, P. Huang, S. Chang, Y.H. Hu, Q. Yang, L.F. Mao, H.M. Yang, Emerging nanoclay composite for effective hemostasis, Adv. Funct. Mater. 28 (10) (2018), 1704452, https://doi.org/10.1002/adfm.201704452. ARTN 1704452.

[8] C. Wang, H. Zhou, H. Niu, X. Ma, Y. Yuan, H. Hong, C. Liu, Tannic acid-loaded mesoporous silica for rapid hemostasis and antibacterial activity, Biomater. Sci. 6 (12) (2018) 3318–3331, https://doi.org/10.1039/c8bm00837j.

[9] Y. Huang, X. Zhao, Z.Y. Zhang, Y.P. Liang, Z.H. Yin, B.J. Chen, L. Bai, Y. Han, B. L. Guo, Degradable gelatin-based IPN cryogel hemostat for rapidly stopping deep noncompressible hemorrhage and simultaneously improving wound healing, Chem. Mater. 32 (15) (2020) 6595–6610, https://doi.org/10.1021/acs.chemmater.0c02030.

[10] C. Wang, H. Niu, X. Ma, H. Hong, Y. Yuan, C. Liu, Bioinspired, injectable, quaternized hydroxyethyl cellulose composite hydrogel coordinated by mesocellular silica foam for rapid, noncompressible hemostasis and wound healing, ACS Appl. Mater. Interfaces 11 (38) (2019) 34595–34608, https://doi.org/10.1021/acsami.9b08799.

[11] X. Yan, W.W. Fang, J. Xue, T.C. Sun, L. Dong, Z. Zha, H. Qian, Y.H. Song, M. Zhang, X. Gong, Y. Lu, T. He, Thermoresponsive in situ forming hydrogel with sol-gel irreversibility for effective methicillin-resistant Staphylococcus aureus infected wound healing, ACS Nano 13 (9) (2019) 10074–10084, https://doi.org/10.1021/acsnano.9b02845.

[12] Q. Peng, J. Chen, Z. Zeng, T. Wang, L. Xiang, X. Peng, J. Liu, H. Zeng, Adhesive coacervates driven by hydrogen-bonding interaction, Small 16 (43) (2020), e2004132, https://doi.org/10.1002/smll.202004132.

[13] X. Zhao, Y. Liang, Y. Huang, J. He, Y. Han, B. Guo, Physical double-network hydrogel adhesives with rapid shape adaptability, fast self-healing, antioxidant and NIR/pH stimulus-responsiveness for multidrug-resistant bacterial infection and removable wound dressing, Adv. Funct. Mater. 30 (17) (2020), https://doi.org/10.1002/adfm.201910748.

[14] J.Y. Liu, Y. Li, Y. Hu, G. Cheng, E. Ye, C. Shen, F.J. Xu, Hemostatic porous sponges of cross-linked hyaluronic acid/cationized dextran by one self-foaming process, Mater. Sci. Eng. C. Mate.r Biol .Appl. 83 (2018) 160–168, https://doi.org/10.1016/j.msec.2017.10.007.

[15] J. Zhou, Y. Wu, X. Zhang, J. Lai, Y. Li, J. Xing, L. Teng, J. Chen, Enzyme catalyzed hydrogel as versatile bioadhesive for tissue wound hemostasis, bonding, and continuous repair, Biomacromolecules 22 (4) (2021) 1346–1356, https://doi.org/10.1021/acs.biomac.0c01329.

[16] H. Yang, L. Song, Y. Zou, D. Sun, L. Wang, Z. Yu, J. Guo, Role of hyaluronic acids and potential as regenerative biomaterials in wound healing, ACS Appl. Bio. Mater. 4 (1) (2021) 311–324, https://doi.org/10.1021/acsabm.0c01364.

[17] J. Zhu, F. Li, X. Wang, J. Yu, D. Wu, Hyaluronic acid and polyethylene glycol hybrid hydrogel encapsulating nanogel with hemostasis and sustainable antibacterial property for wound healing, ACS Appl. Mater. Interfaces 10 (16) (2018) 13304–13316, https://doi.org/10.1021/acsami.7b18927.

[18] Y. Okamura, S. Katsuno, H. Suzuki, H. Maruyama, M. Handa, Y. Ikeda, S. Takeoka, Release abilities of adenosine diphosphate from phospholipid vesicles with different membrane properties and their hemostatic effects as a platelet substitute, J. Contr. Release 148 (3) (2010) 373–379, https://doi.org/10.1016/j.jconrel.2010.09.013.

[19] E.M. Golebiewska, A.W. Poole, Platelet secretion: from haemostasis to wound healing and beyond, Blood Rev. 29 (3) (2015) 153–162, https://doi.org/10.1016/j.blre.2014.10.003.

[20] C.C. Baaten, L.F. Veenstra, R. Wetzels, J.P. van Geffen, F. Swieringa, S.M. de Witt, Y.M. Henskens, H. Crijns, S. Nylander, J.J. van Giezen, J.W. Heemskerk, P.E. van der Meijden, Gradual increase in thrombogenicity of juvenile platelets formed upon offset of prasugrel medication, Haematologica 100 (9) (2015) 1131–1138, https://doi.org/10.3324/haematol.2014.122457.

[21] X. Wang, J. Guan, X. Zhuang, Z. Li, S. Huang, J. Yang, C. Liu, F. Li, F. Tian, J. Wu, Z. Shu, Exploration of blood coagulation of N-alkyl chitosan nanofiber membrane in vitro, Biomacromolecules 19 (3) (2018) 731–739, https://doi.org/10.1021/acs.biomac.7b01492.

[22] P. Choudhary, B. Ramalingam, S.K. Das, Fabrication of chitosan-reinforced multifunctional graphene nanocomposite as antibacterial scaffolds for hemorrhage control and wound-healing application, ACS Biomater. Sci. Eng. 6 (10) (2020) 5911–5929, https://doi.org/10.1021/acsbiomaterials.0c00923.

[23] G.P. Chen, Y.R. Yu, X.W. Wu, G.F. Wang, J.N. Ren, Y.J. Zhao, Bioinspired multifunctional hybrid hydrogel promotes wound healing, Adv. Funct. Mater. 28 (33) (2018), 1801386, https://doi.org/10.1002/adfm.201801386. ARTN 1801386.

[24] D.T. Vo, C.K. Lee, Antimicrobial sponge prepared by hydrophobically modified chitosan for bacteria removal, Carbohydr. Polym. 187 (2018) 1–7, https://doi.org/10.1016/j.carbpol.2018.01.082.

[25] M.B. Dowling, R. Kumar, M.A. Keibler, J.R. Hess, G.V. Bochicchio, S.R. Raghavan, A self-assembling hydrophobically modified chitosan capable of reversible hemostatic action, Biomaterials 32 (13) (2011) 3351–3357, https://doi.org/10.1016/j.biomaterials.2010.12.033.

[26] X. Yang, C. Wang, Y. Liu, H. Niu, W. Zhao, J. Wang, K. Dai, Inherent antibacterial and instant swelling epsilon-poly-lysine/poly(ethylene glycol) diglycidyl ether superabsorbent for rapid hemostasis and bacterially infected wound healing, ACS Appl. Mater. Interfaces 13 (31) (2021) 36709–36721, https://doi.org/10.1021/acsami.1c02421.

[27] Y.L. Wong, L. LeBon, A.M. Basso, K.L. Kohlhaas, A.L. Nikkel, H.M. Robb, D. L. Donnelly-Roberts, J. Prakash, A.M. Swensen, N.D. Rubinstein, S. Krishnan, F. E. McAllister, N.V. Haste, J.J. O'Brien, M. Roy, A. Ireland, J.M. Frost, L. Shi, S. Riedmaier, K. Martin, M.J. Dart, C. Sidrauski, eIF2B activator prevents neurological defects caused by a chronic integrated stress response, Elife 8 (2019), https://doi.org/10.7554/eLife.42940.

[28] A. Paschalis, B. Sheehan, R. Riisnaes, D.N. Rodrigues, B. Gurel, C. Bertan, A. Ferreira, M.B.K. Lambros, G. Seed, W. Yuan, D. Dolling, J.C. Welti, A. Neeb, S. Sumanasuriya, P. Rescigno, D. Bianchini, N. Tunariu, S. Carreira, A. Sharp, W. Oyen, J.S. de Bono, Prostate-specific membrane antigen heterogeneity and DNA repair defects in prostate cancer, Eur. Urol. 76 (4) (2019) 469–478, https://doi.org/10.1016/j.eururo.2019.06.030.

[29] R. Guo, L.D. Berry, D.L. Aisner, J. Sheren, T. Boyle, P.A. Bunn Jr., B.E. Johnson, D. J. Kwiatkowski, A. Drilon, L.M. Sholl, M.G. Kris, MET IHC is a poor screen for MET amplification or MET exon 14 mutations in lung adenocarcinomas: data from a tri-institutional cohort of the lung cancer mutation consortium, J. Thorac. Oncol. 14 (9) (2019) 1666–1671, https://doi.org/10.1016/j.jtho.2019.06.009.

[30] P. Luo, L. Liu, W. Xu, L. Fan, M. Nie, Preparation and characterization of aminated hyaluronic acid/oxidized hydroxyethyl cellulose hydrogel, Carbohydr. Polym. 199 (2018) 170–177, https://doi.org/10.1016/j.carbpol.2018.06.065.

[31] M. Okawa, M. Sakoda, S. Ohta, K. Hasegawa, Y. Yatomi, T. Ito, The balance between the hemostatic effect and immune response of hyaluronan conjugated with different chain lengths of inorganic polyphosphate, Biomacromolecules 21 (7) (2020) 2695–2704, https://doi.org/10.1021/acs.biomac.0c00390.

[32] M. Sakoda, M. Kaneko, S. Ohta, P. Qi, S. Ichimura, Y. Yatomi, T. Ito, Injectable hemostat composed of a polyphosphate-conjugated hyaluronan hydrogel, Biomacromolecules 19 (8) (2018) 3280–3290, https://doi.org/10.1021/acs.biomac.8b00588.

[33] X. Liu, Q. Zhang, Z. Gao, R. Hou, G. Gao, Bioinspired adhesive hydrogel driven by adenine and thymine, ACS Appl. Mater. Interfaces 9 (20) (2017) 17645–17652, https://doi.org/10.1021/acsami.7b04832.

[34] Q. Chen, Y. Liu, T. Wang, J. Wu, X. Zhai, Y. Li, W.W. Lu, H. Pan, X. Zhao, Chitosan-PVA monodisperse millimeter-sized spheres prepared by electrospraying reduce the thromboembolic risk in hemorrhage control, J. Mater. Chem. B 5 (20) (2017) 3686–3696, https://doi.org/10.1039/c7tb00032d.

[35] R. Saud, S. Pokhrel, P.N. Yadav, Synthesis, characterization and antimicrobial activity of maltol functionalized chitosan derivatives, J. Macromol. Sci., Pure Appl. Chem. 56 (4) (2019) 375–383, https://doi.org/10.1080/10601325.2019.1578616.

[36] H. Choudhary, M.B. Rudy, M.B. Dowling, S.R. Raghavan, Foams with enhanced rheology for stopping bleeding, ACS Appl. Mater. Interfaces 13 (12) (2021) 13958–13967, https://doi.org/10.1021/acsami.0c22818.

[37] J. Zhu, T. Xiao, J. Zhang, H. Che, Y. Shi, X. Shi, J.C.M. van Hest, Surface-charge-switchable nanoclusters for magnetic resonance imaging-guided and glutathione depletion-enhanced photodynamic therapy, ACS Nano 14 (9) (2020) 11225–11237, https://doi.org/10.1021/acsnano.0c03080.

[38] Y. Liang, M. Li, Y. Huang, B. Guo, An integrated strategy for rapid hemostasis during tumor resection and prevention of postoperative tumor recurrence of hepatocellular carcinoma by antibacterial shape memory cryogel, Small 17 (38) (2021), e2101356, https://doi.org/10.1002/smll.202101356.

[39] L. Wang, Y. Zhong, C. Qian, D. Yang, J. Nie, G. Ma, A natural polymer-based porous sponge with capillary-mimicking microchannels for rapid hemostasis, Acta Biomater. 114 (2020) 193–205, https://doi.org/10.1016/j.actbio.2020.07.043.

[40] J. Zhu, H. Han, F.X. Li, X.L. Wang, J.Y. Yu, X.H. Qin, D.Q. Wu, Peptide-Functionalized amino acid-derived pseudoprotein-based hydrogel with hemorrhage control and antibacterial activity for wound healing, Chem. Mater. 31 (12) (2019) 4436–4450, https://doi.org/10.1021/acs.chemmater.9b00850.

[41] P. Lou, S. Liu, X. Xu, C. Pan, Y. Lu, J. Liu, Extracellular vesicle-based therapeutics for the regeneration of chronic wounds: current knowledge and future perspectives, Acta Biomater. 119 (2021) 42–56, https://doi.org/10.1016/j.actbio.2020.11.001.

[42] Z. Li, S. Hu, K. Cheng, Platelets and their biomimetics for regenerative medicine and cancer therapies, J. Mater. Chem. B 6 (45) (2018) 7354–7365, https://doi.org/10.1039/C8TB02301H.

[43] S. Pourshahrestani, N.A. Kadri, E. Zeimaran, M.R. Towler, Well-ordered mesoporous silica and bioactive glasses: promise for improved hemostasis, Biomater. Sci. 7 (1) (2018) 31–50, https://doi.org/10.1039/c8bm01041b.

[44] X. Xie, D. Li, Y. Chen, Y. Shen, F. Yu, W. Wang, Z. Yuan, Y. Morsi, J. Wu, X. Mo, Conjugate electrospun 3D gelatin nanofiber sponge for rapid hemostasis, Adv. Healthc. Mater. 10 (20) (2021), e2100918, https://doi.org/10.1002/adhm.202100918.

[45] Y. Yang, Y. Liang, J. Chen, X. Duan, B. Guo, Mussel-inspired adhesive antioxidant antibacterial hemostatic composite hydrogel wound dressing via photo-polymerization for infected skin wound healing, Bioact. Mater. 8 (2022) 341–354, https://doi.org/10.1016/j.bioactmat.2021.06.014.

[46] W. Huang, Y. Wang, Z. Huang, X. Wang, L. Chen, Y. Zhang, L. Zhang, On-demand dissolvable self-healing hydrogel based on carboxymethyl chitosan and cellulose nanocrystal for deep partial thickness burn wound healing, ACS Appl. Mater. Interfaces 10 (48) (2018) 41076–41088, https://doi.org/10.1021/acsami.8b14526.

[47] M.M. Rahman, N. Garcia, Y.S. Loh, D.C. Marks, I. Banakh, P. Jagadeesan, N. R. Cameron, C. Yung-Chih, M. Costa, K. Peter, H. Cleland, S. Akbarzadeh, A platelet-derived hydrogel improves neovascularisation in full thickness wounds, Acta Biomater. 136 (2021) 199–209, https://doi.org/10.1016/j.actbio.2021.09.043.

[48] B.Z. Johnson, A.W. Stevenson, C.M. Prele, M.W. Fear, F.M. Wood, The role of IL-6 in skin fibrosis and cutaneous wound healing, Biomedicines 8 (5) (2020), https://doi.org/10.3390/biomedicines8050101.

[49] M.H. Kim, F. Gorouhi, S. Ramirez, J.L. Granick, B.A. Byrne, A.M. Soulika, S. I. Simon, R.R. Isseroff, Catecholamine stress alters neutrophil trafficking and impairs wound healing by beta2-adrenergic receptor-mediated upregulation of IL-6, J. Invest. Dermatol. 134 (3) (2014) 809–817, https://doi.org/10.1038/jid.2013.415.